Supplements:

S1.1 Instrumental

S1.1.1 Diode Laser

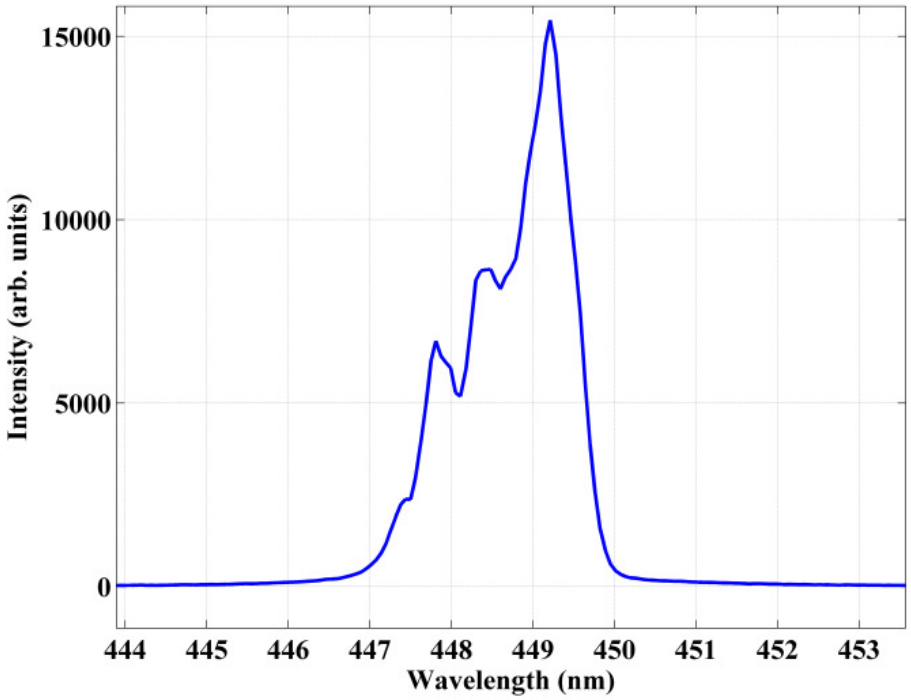

Fig. S1: Wavelength plot for the diode laser, operated with repetition rate of 5MHz. The wavelength of the diode laser is measured with a spectrometer[1].

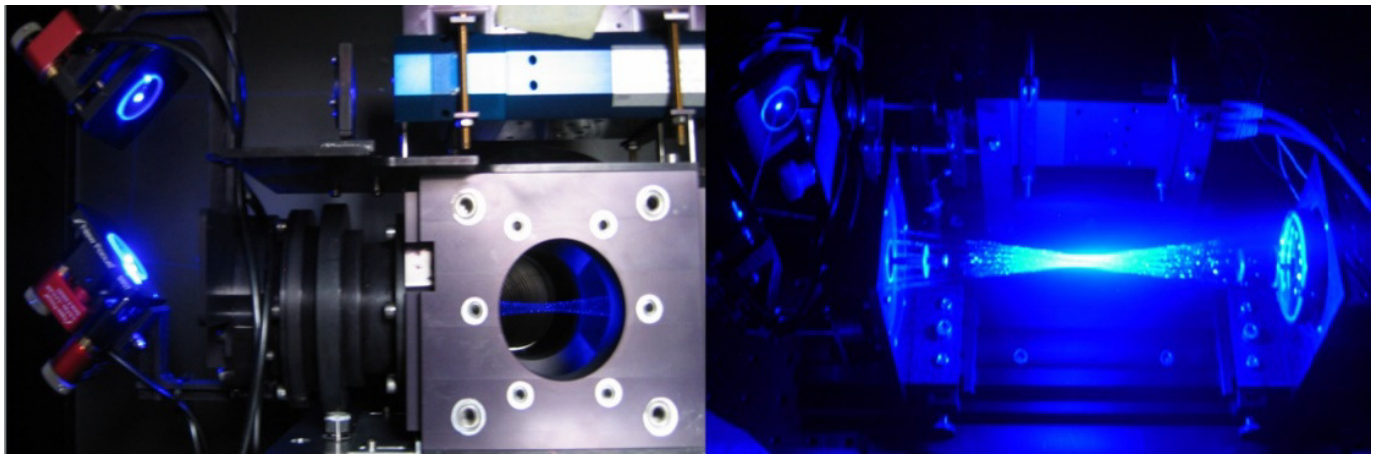

Fig. S2: Multiple passes of the laser beam are visible in the detection cell (left) and in between the Herriott cell's mirrors on an optical bench (right).

[1] HR4000 High-Resolution Spectrometer, Ocean Optics, USA

S1.1.2 ON-OFF Laser cycle simulation

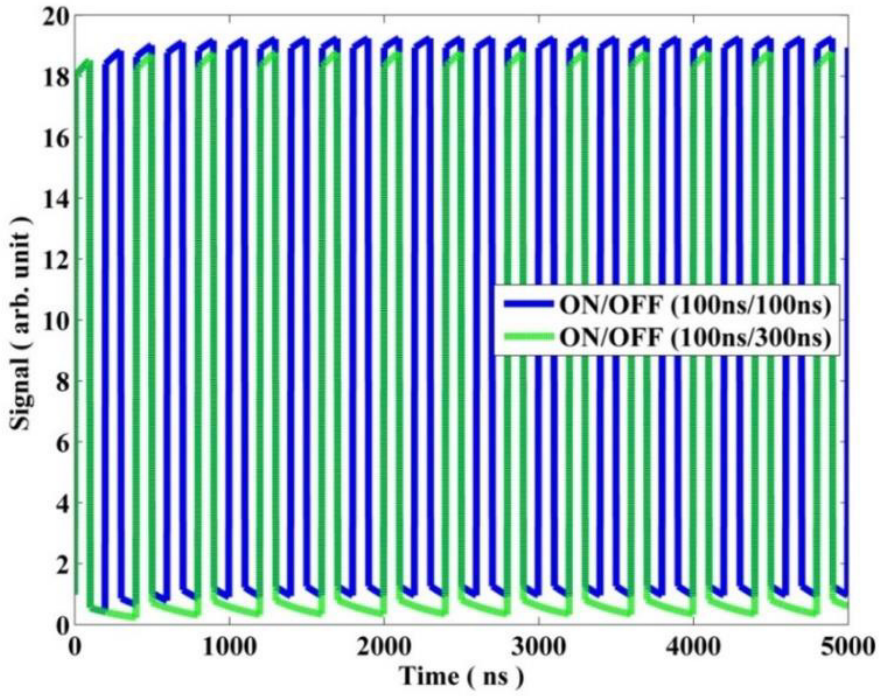

Fig. S3: Simulated ON/OFF cycles for operating the diode-lase

S1.1.3 Laser ON/OFF cycle

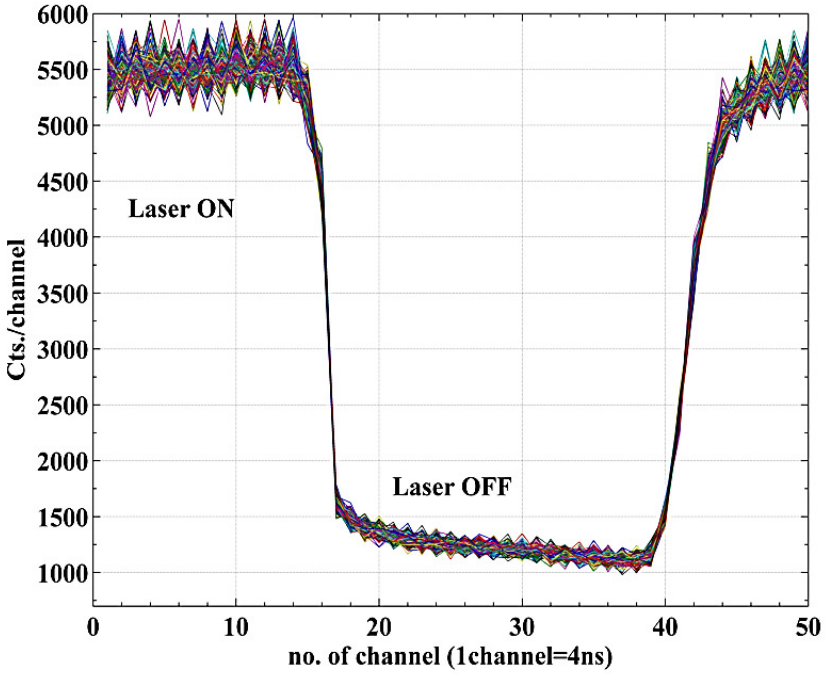

Fig. S4: 200ns on-off cycle of laser for a signal (~12ppb$_v$ NO_2) [y-axis arb. unit]

S1.1.4 Reactions for calibration simulations

Note; all reactions and rate coefficients from k1 to k64 are taken from (Atkinson et al., 2004) except k54 (temperature dependent) from (Sander et al., 2011). The impact of the difference between the JPL and IUPAC rate constant is less than 1 % on our results.

k1	:	$O + O_2$	=	O_3;
k25	:	$OH + O_3$	=	$HO_2 + O_2$;
k28	:	$HO_2 + O_3$	=	$OH + O_2 + O_2$;
k31	:	$O + NO$	=	NO_2;
k32	:	$O + NO_2$	=	$O_2 + NO$;
k33	:	$O + NO_2$	=	NO_3;
k34	:	$O + NO_3$	=	$O_2 + NO_2$;
k39	:	$OH + HONO$	=	$H_2O + NO_2$;
k40	:	$OH + HNO_3$	=	$H_2O + NO_3$;
k41	:	$OH + HNO_4$	=	products;
k42	:	$OH + NO$	=	HONO;
k43	:	$OH + NO_2$	=	HNO_3;
k44	:	$OH + NO_3$	=	$HO_2 + NO_2$;
k45	:	$HO_2 + NO$	=	$OH + NO_2$;
k46	:	$HO_2 + NO_2$	=	HNO_4;
k47	:	HNO_4	=	$HO_2 + NO_2$;
k48	:	$HO_2 + NO_3$	=	products;
k53	:	$NO + NO + O_2$	=	$NO_2 + NO_2$;
k54	:	$NO + O_3$	=	$NO_2 + O_2$;
k55	:	$NO + NO_2$	=	N_2O_3;
k56	:	N_2O_3	=	$NO + NO_2$;
k57	:	$NO + NO_3$	=	$NO_2 + NO_2$;
k58	:	$NO_2 + O_3$	=	$NO_3 + O_2$;
k59	:	$NO_2 + NO_2$	=	N_2O_4;
k60	:	N_2O_4	=	$NO_2 + NO_2$;
k61	:	$NO_2 + NO_3$	=	N_2O_5;
k62	:	N_2O_5	=	$NO_2 + NO_3$;
k63	:	$N_2O_5 + H_2O$	=	$HNO_3 + HNO_3$;
k64	:	$N_2O_5 + H_2O + H_2O$	=	$HNO_3 + H_2O$;

S1.1.5 Box Model simulated temperature and pressure effect on calibrator

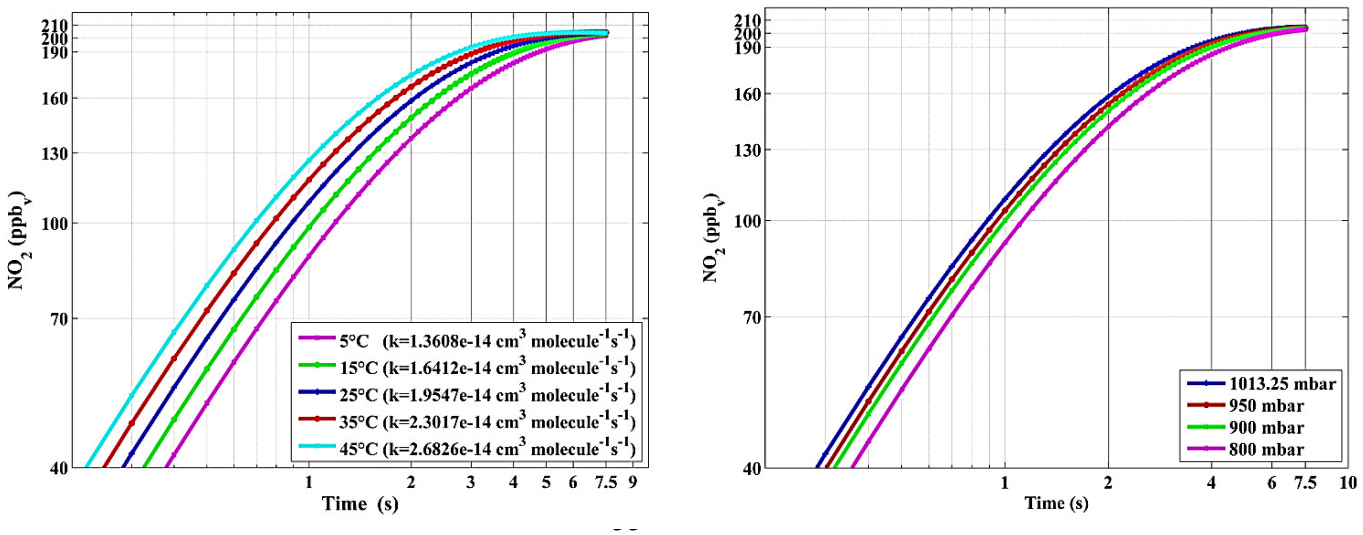

Fig. S5: In the left panel, NO_2 concentrations inside the calibrator as a function of time based on different temperatures. While the right panel shows NO_2 concentrations inside the calibrator as a function of time for different pressures (mbar or hPa).

60

S1.1.6 Gas phase titration NO_{GPT}

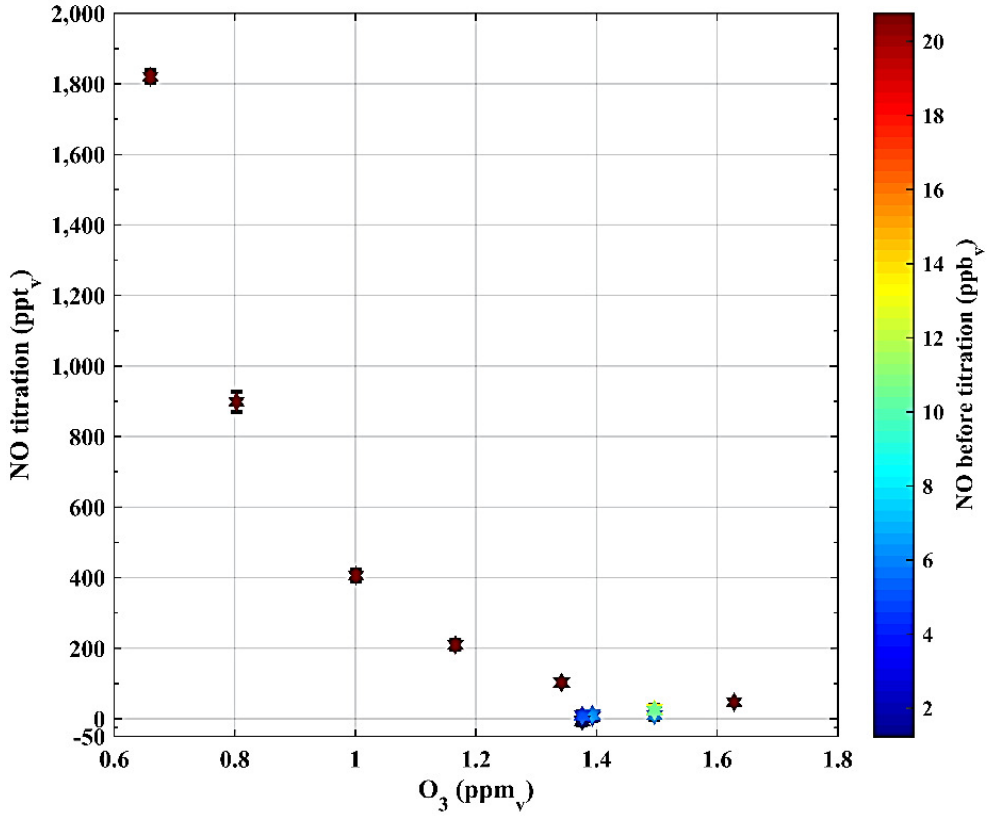

Fig. S6: NO_{GPT} based on a CLD measurements as a function of the reaction chamber O_3 mixing ratios.

S1.1.7 Limit of Detection

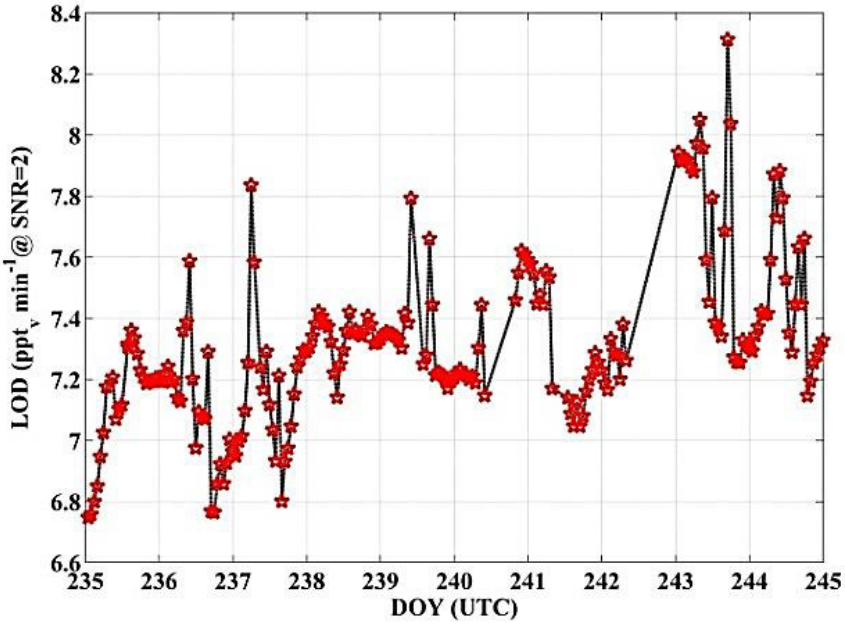

Fig. S7: An example for the limit of detection of GANDALF based on different calibrations, taken from an automated calibrated period of PARADE-2011 according to the Eq. 4 (Section 2.3) in the main draft.

S1.2 PARADE-2011

S1.2.1 Air Mass Origin

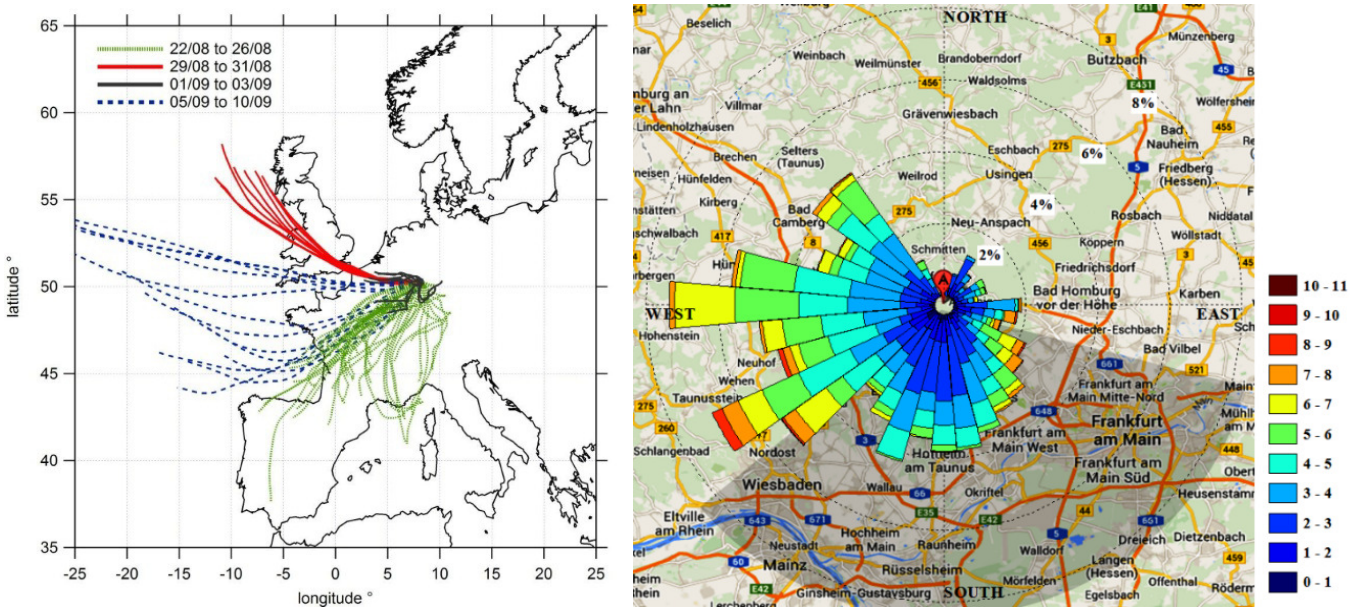

Fig. S8: Origin of air mass for PARADE-2011 [Figure is taken from Crowley, J., 2012 (left)]. Frequency distributions of wind directions with wind speed (colour-coded: wind speed in ms^{-1}). [Google Map view (www.google.com/maps)]. While shaded area in R.H.S is showing possible anthropogenic influence from nearby cities.

S1.2.2 Frequency plot of NO_2 measurements

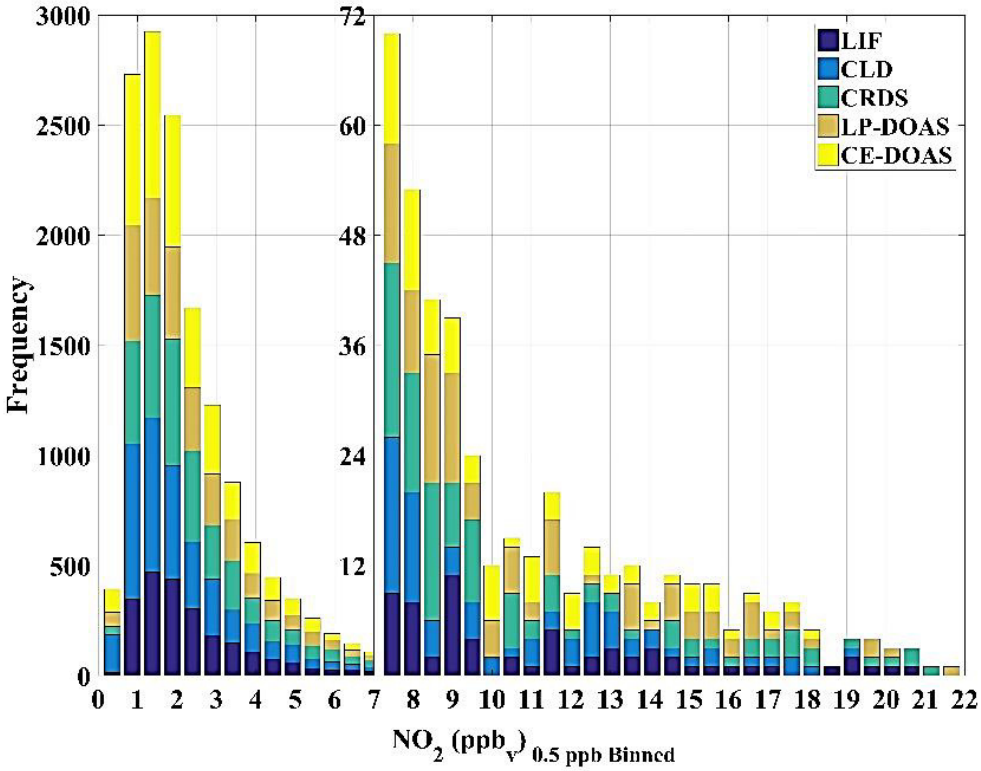

Fig. S9: Histogram of the distribution of the data for different NO_2 measurements during PARADE 2011.

S1.2.3 Time series of NO_2 measurements

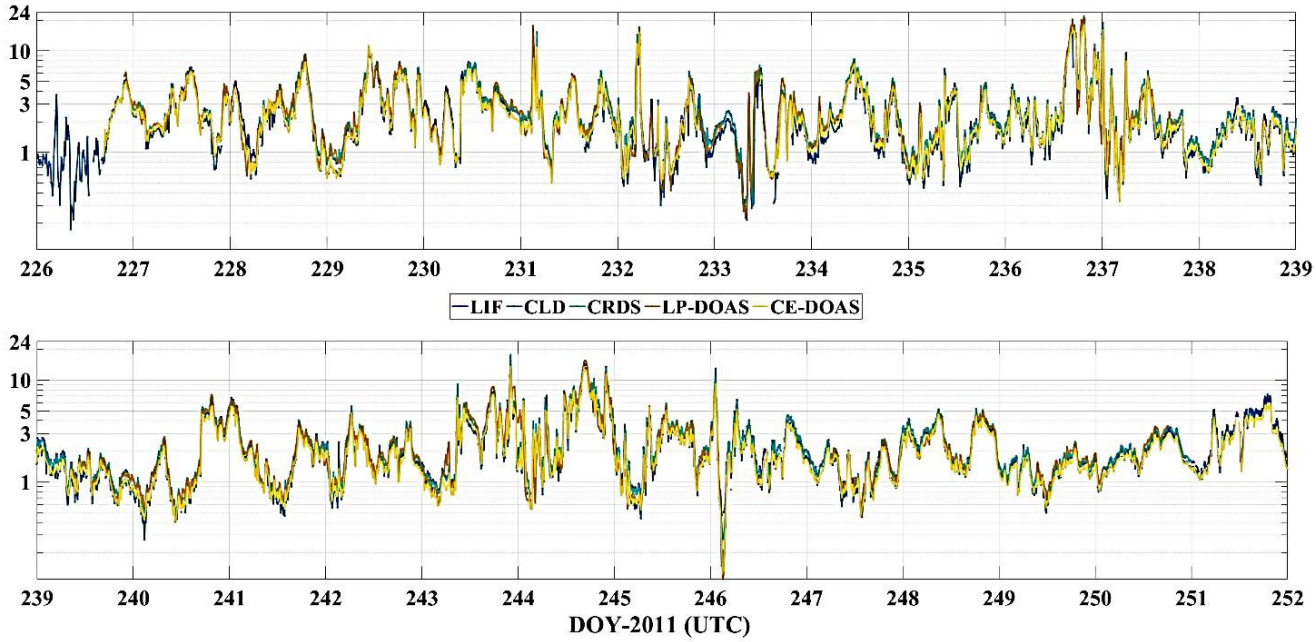

Fig. S10: PARADE 2011 time series (10 min. averages) of NO_2 observations (y-axis in ppb_v) based on different instruments.

S1.2.4 Individual correlation with GANDALF (x-axis)

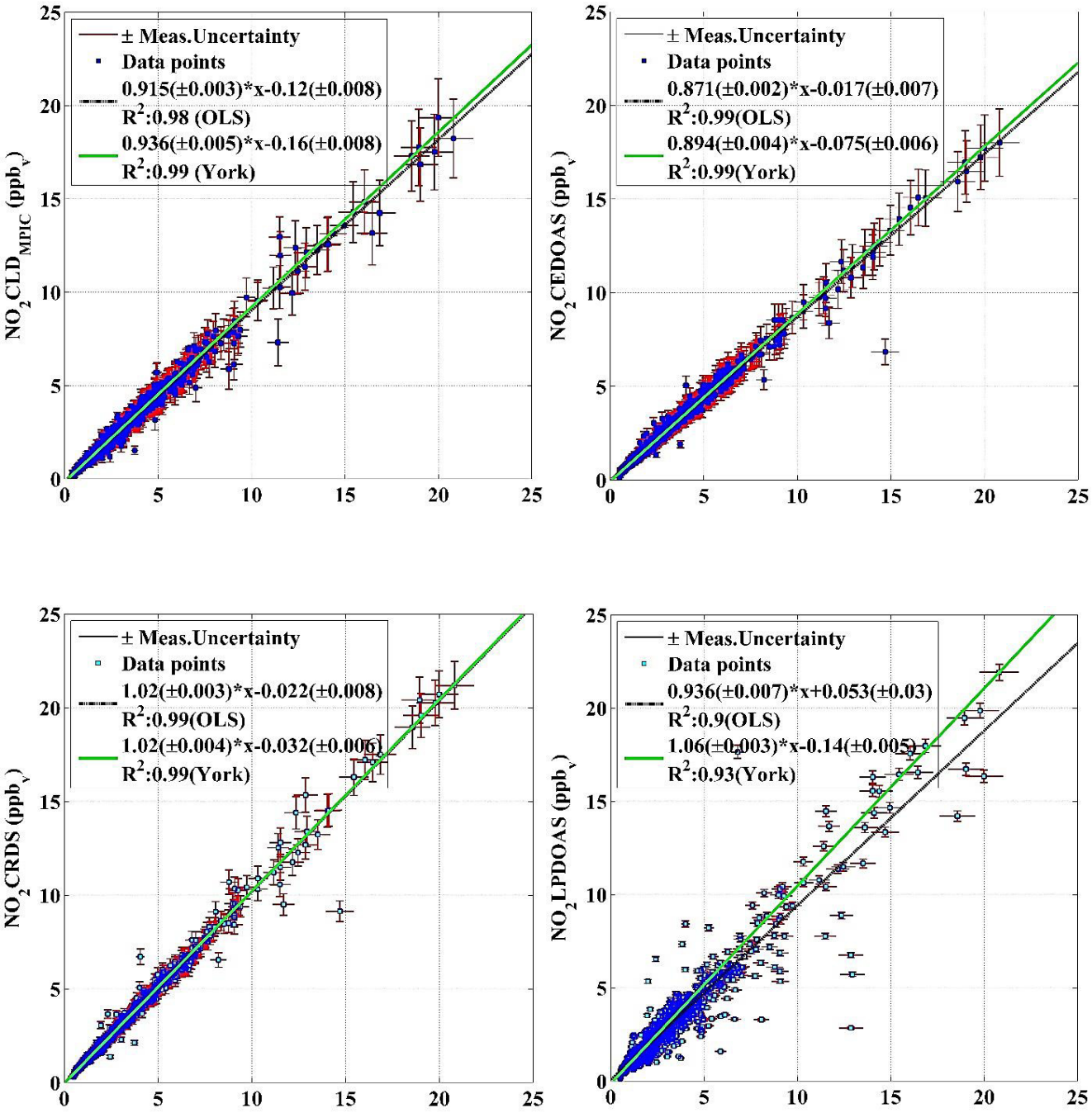

Fig. S11: The individual correlation of different NO_2 instruments (y-axis) versus GANDALF (x-axis) is shown for available 10 minutes data averages. The two different fitting procedures i.e. based on least square fit (Bevington and Robinson, 1992) and York method (York et al., 2004) are applied.

S1.2.5 NO_2 Ratios Correlations

This section is related to NO_2 comparison for PARADE. A series of upcoming figures shows ratio (between all NO_2 measurements and GANDALF) as a function of different observed quantities to see any systematic correlation. Each figure is a set of four subplots according to different instruments. Y-axis of figures below is shown as follow (with data colour to show sequence of upcoming figures for quick go through).

LP-DOAS / GANDALF	**CRDS / GANDALF**
CE-DOAS / GANDALF	**CRD / GANDALF**

Fig. S12: Ratios of different NO_2 measurements with respect to GANDALF as a function of different measured species and parameters based on 10 minute averages.

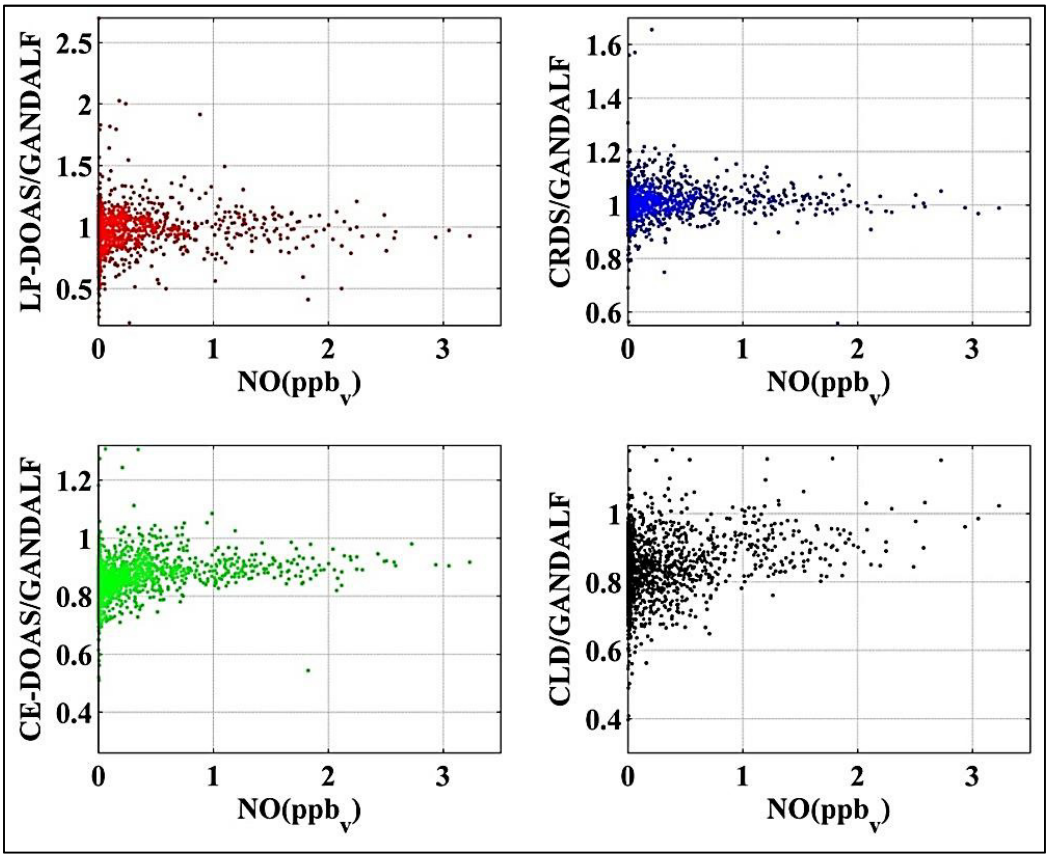

Fig. S12: continue

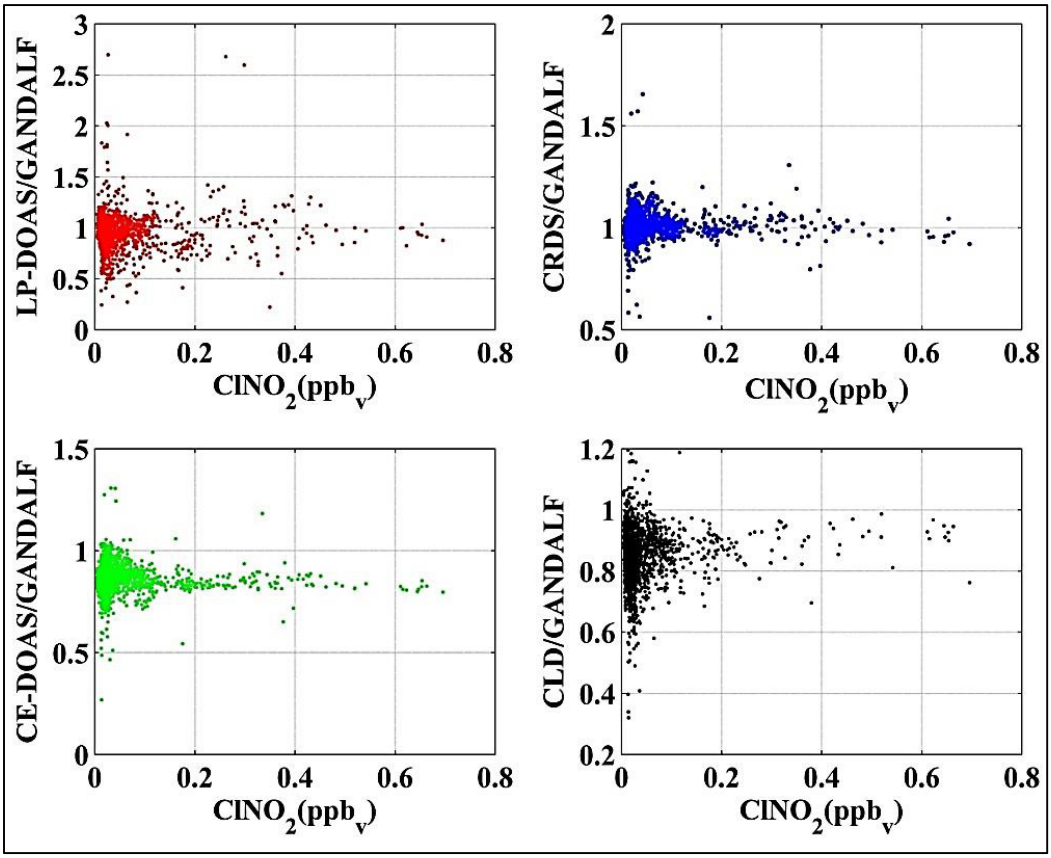

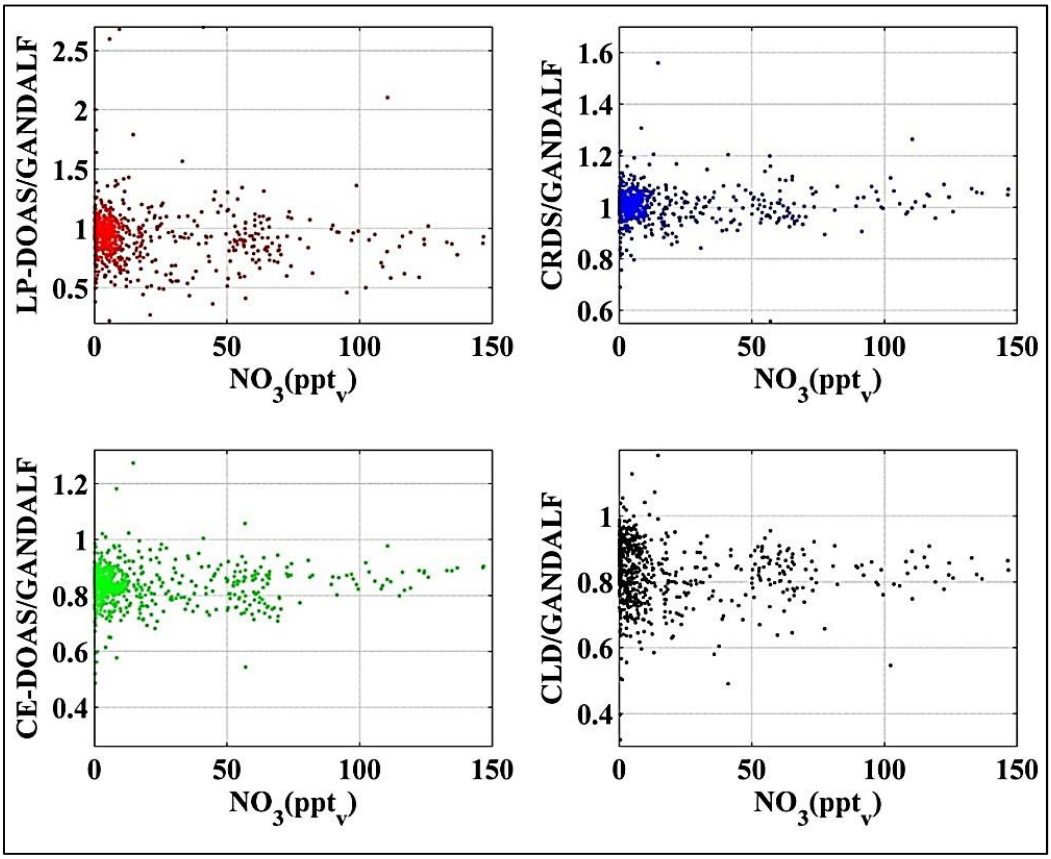

Fig. S12: continue

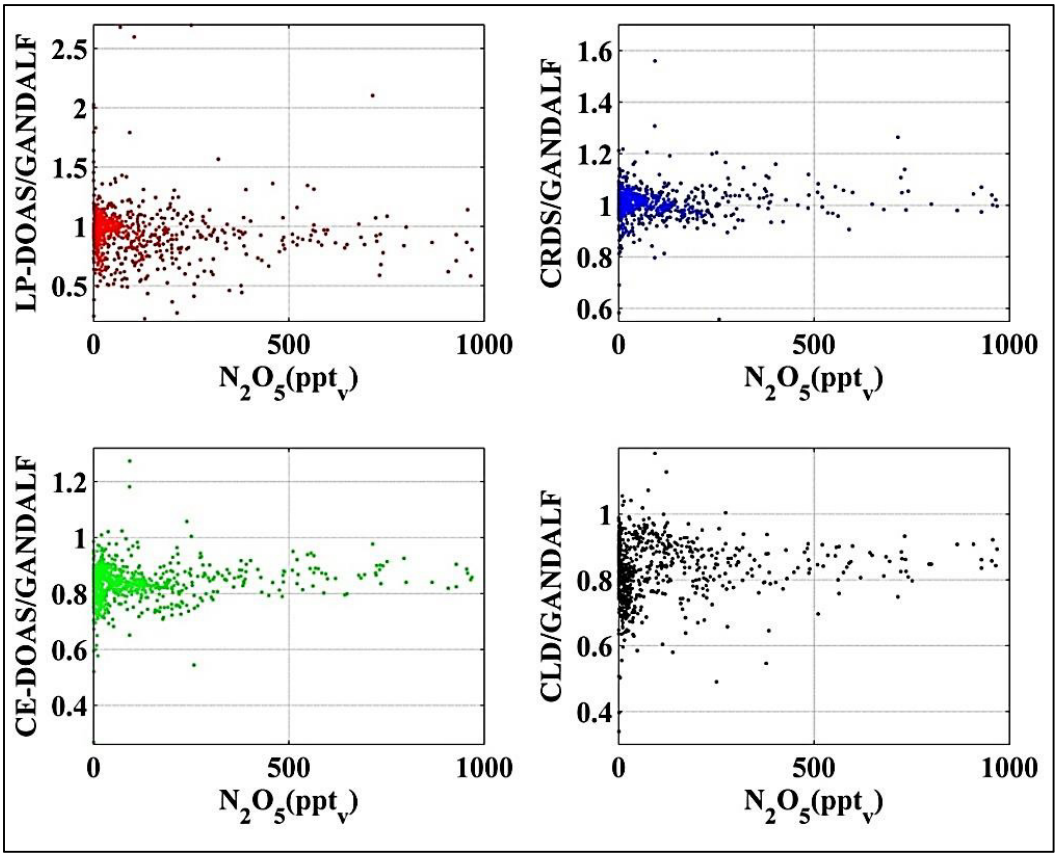

Fig. S12: continue

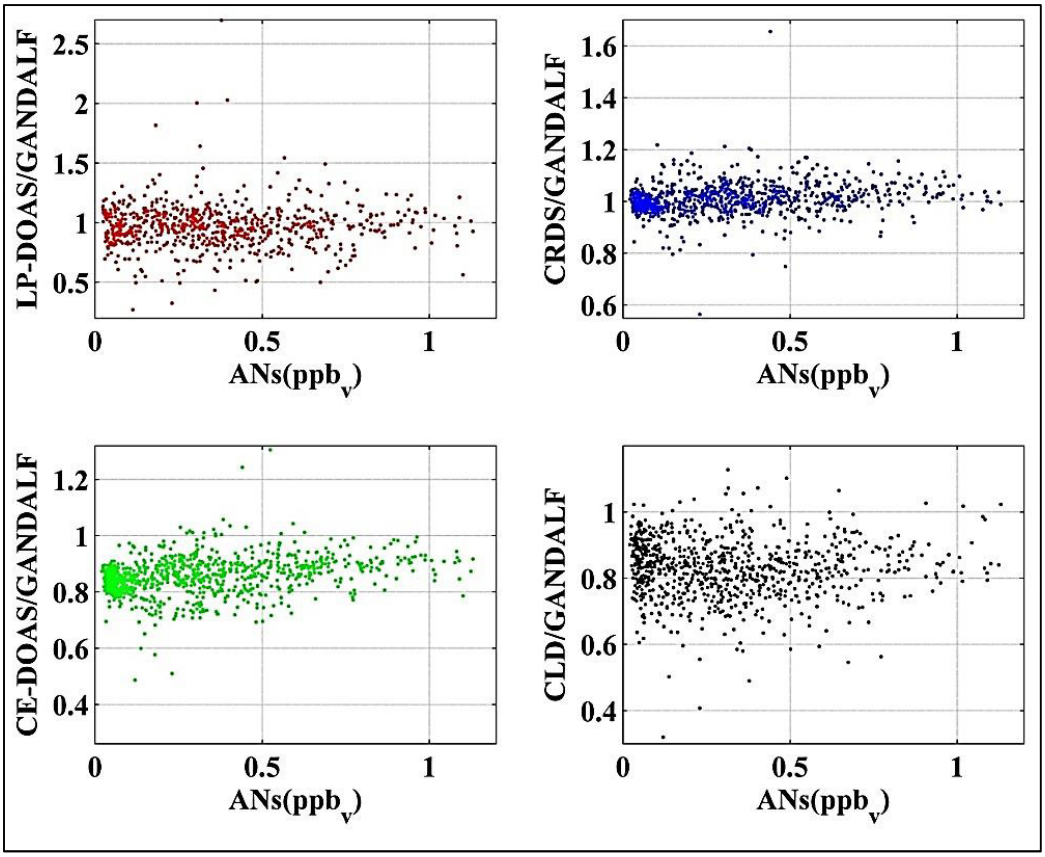

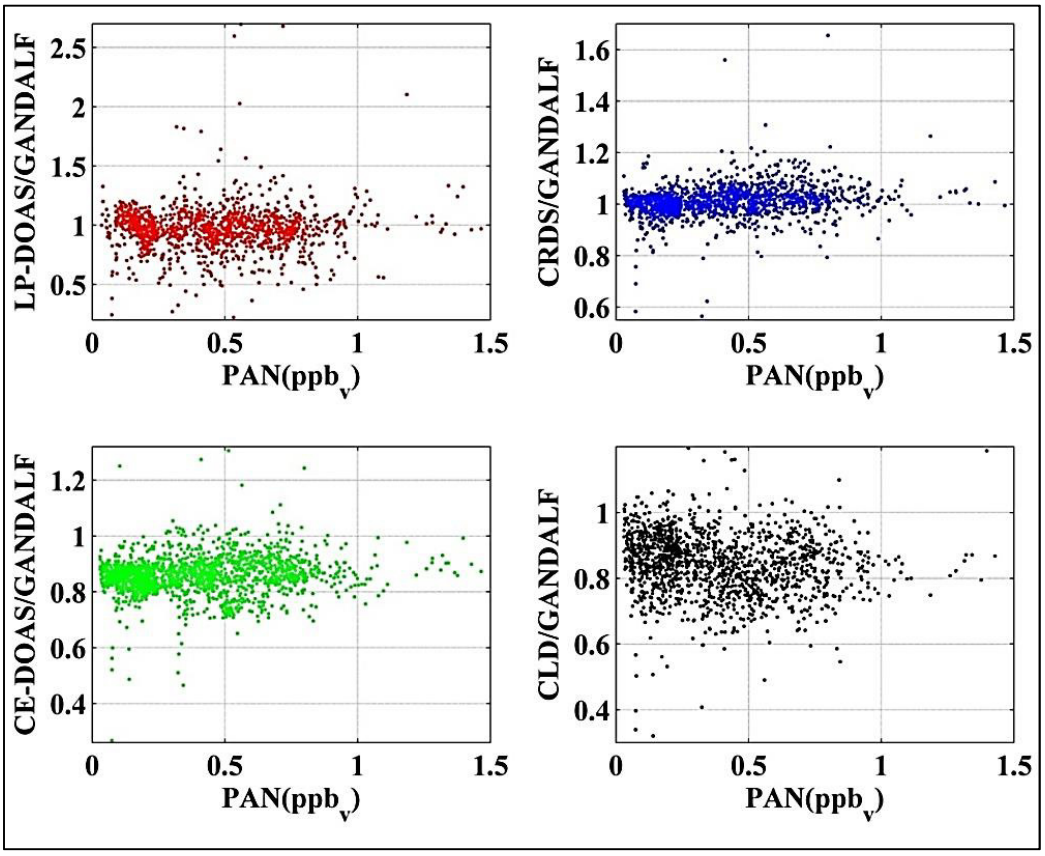

115

Fig. S12: continue

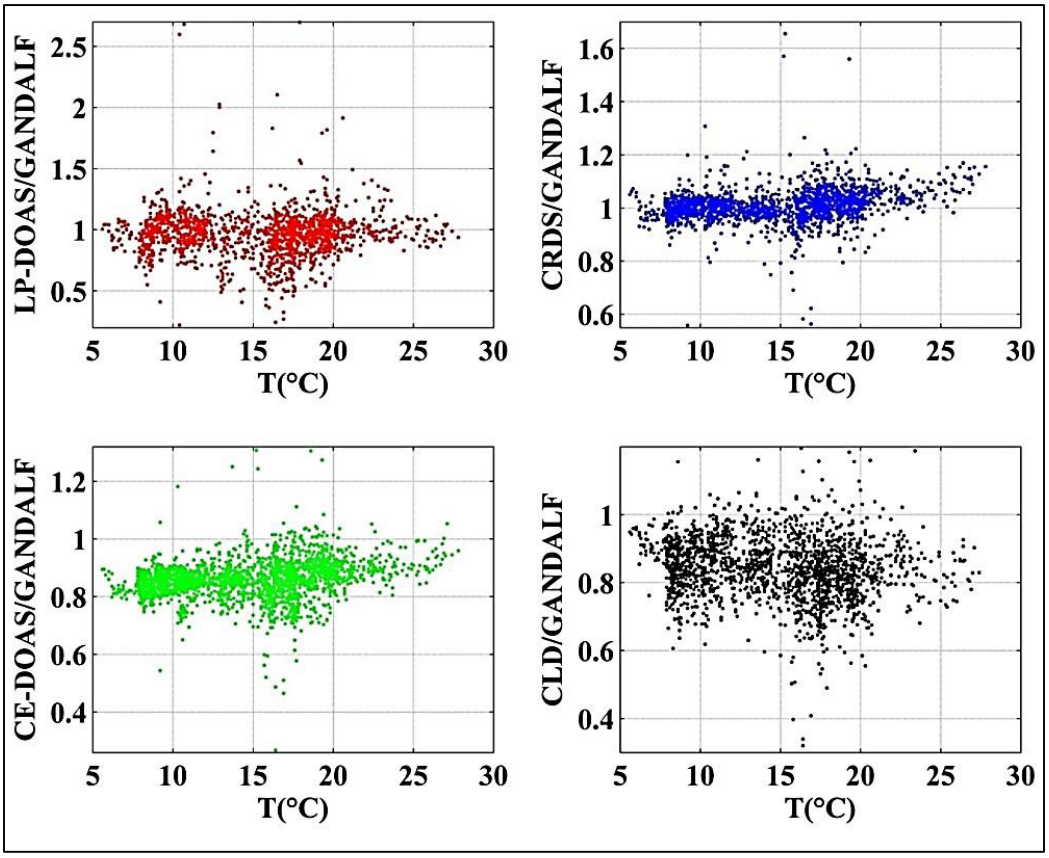

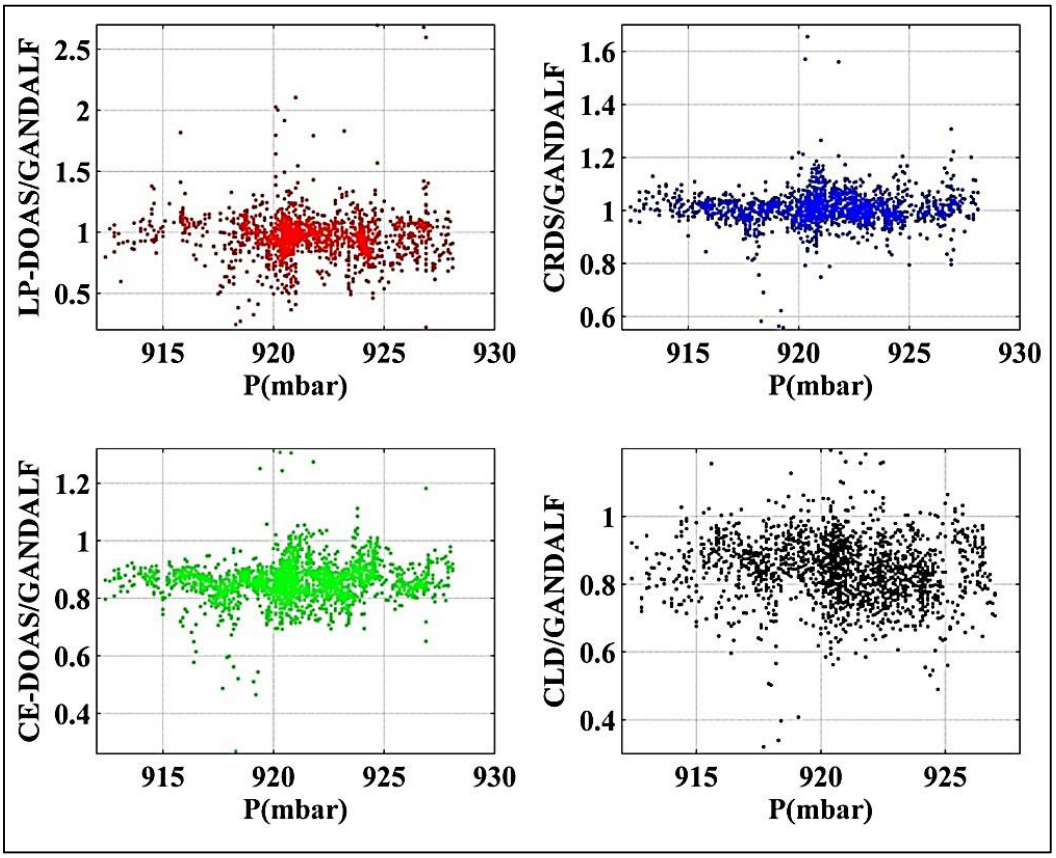

Fig. S12: continue

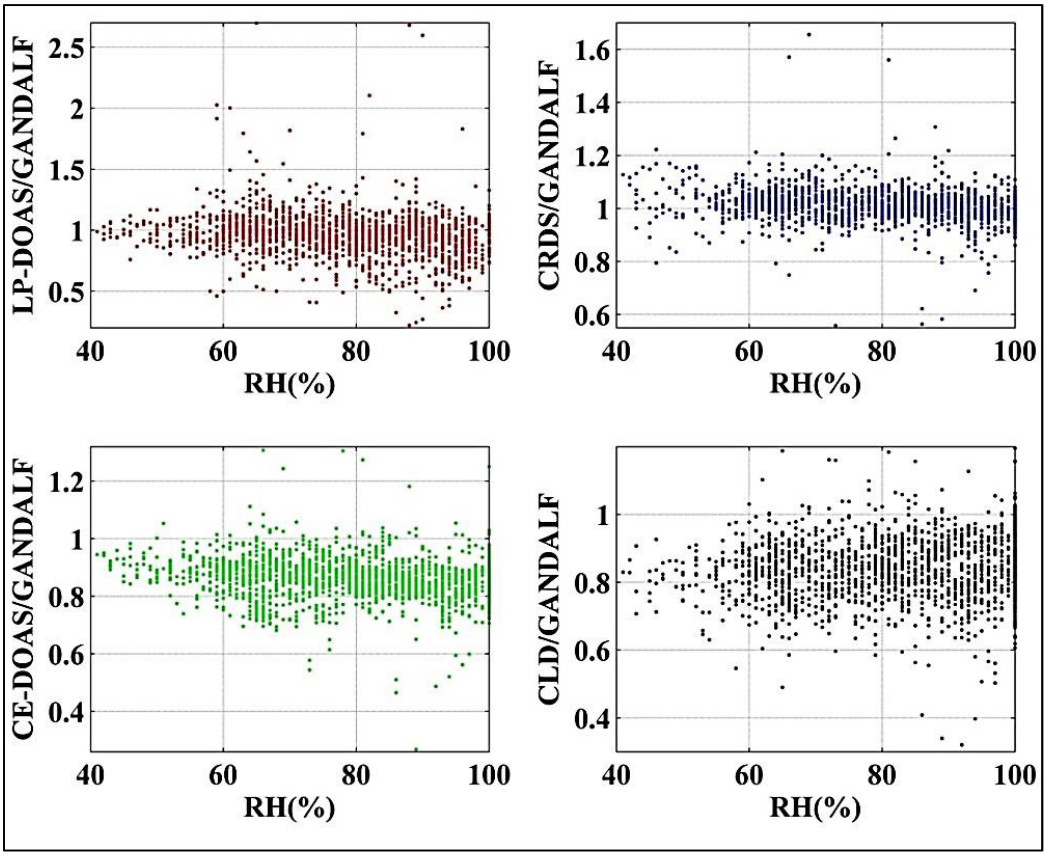

120

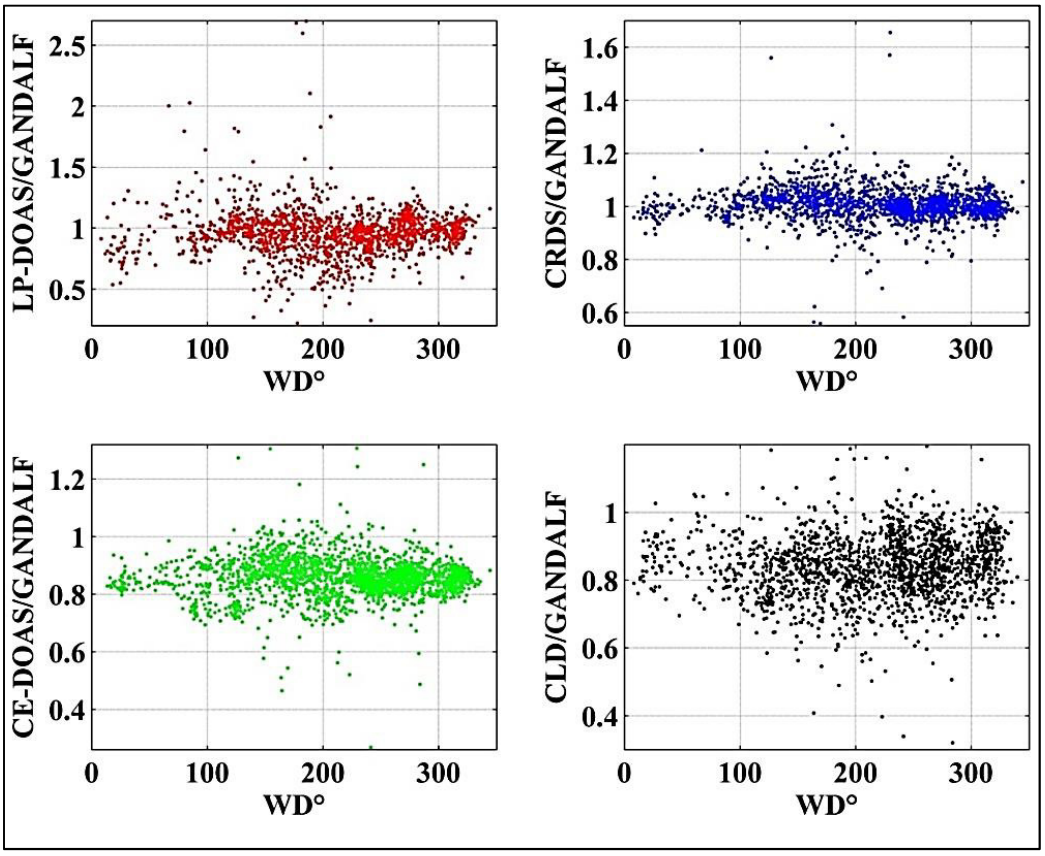

Fig. S12: continue

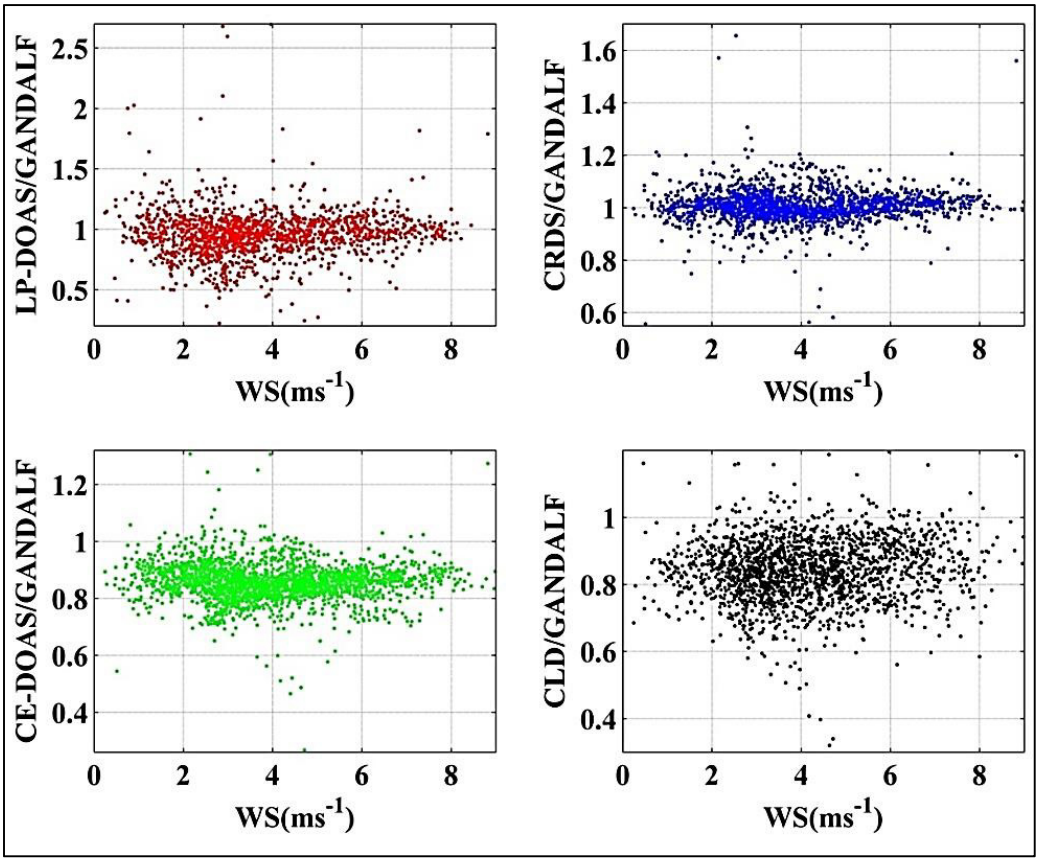

Fig. S12: continue

S1.3 References

Atkinson, R., Baulch, D. L., Cox, R. A., Crowley, J. N., Hampson, R. F., Hynes, R. G., Jenkin, M. E., Rossi, M. J., and Troe, J.: Evaluated kinetic and photochemical data for atmospheric chemistry: Volume I - gas phase reactions of O_x, HO_x, NO_x and SO_x species, Atmos Chem Phys, 4, 1461-1738, 2004.

Bevington, P. R., and Robinson, D. K.: Data reduction and error analysis for the physical sciences, 2nd ed., McGraw-Hill, New York, xvii, 328 p. pp., 1992.

Crowley, J., PArticles and RAdicals: Diel observations of the impact of urban and biogenic Emissions, PARADE data meeting at Max Planck Institute for Chemistry, Mainz, 10th May, 2012.

Sander, S. P., Abbatt, J., Barker, J. R., Burkholder, J. B., Friedl, R. R., Golden, D. M., Huie, R. E., Kolb, C. E., Kurylo, M. J., Moortgat, G. K., Orkin, V. L., and and Wine, P. H.: Chemical Kinetics and Photochemical Data for Use in Atmospheric Studies, in: JPL Publication 10-6, 2011.

York, D., Evensen, N. M., Martinez, M. L., and Delgado, J. D.: Unified equations for the slope, intercept, and standard errors of the best straight line, American Journal of Physics, 72, 367-375, Doi 10.1119/1.1632486, 2004.